

121  
12/11/87 UB  
PPPL-2463  
UC20-G

(2) (5)


PPPL-2463

SAWTOOTH EFFECTS IN INTOR AND TIBER

By

D.P. Stotler, D. Post, and G. Bateman

AUGUST 1987

PLASMA  
PHYSICS  
LABORATORY 

PRINCETON UNIVERSITY  
PRINCETON, NEW JERSEY

PREPARED FOR THE U.S. DEPARTMENT OF ENERGY,  
UNDER CONTRACT DE-AC02-76-CEO-3073.

DISTRIBUTION STATEMENT

## Sawtooth Effects in INTOR and TIBER

D. P. Stotler, D. Post, and Glenn Bateman

### ABSTRACT

Transport simulations of the present designs for the INTOR and TIBER ignition devices predict that broad sawtooth oscillations will appear in these experiments. As was noted previously in studies of the Compact Ignition Tokamak, the primary effect of the oscillations is to reduce fusion power production on the average through profile flattening. Due to the disparate time scales for energy and current diffusion between sawtooth crashes, the simulations also produce peaked pressure profiles over a large low shear region inside the  $q = 1$  surface ( $q$  is the safety factor). Pressure-driven modes will likely be unstable in this case.

### DISCLAIMER

This report was prepared as an account of work sponsored by an agency of the United States Government. Neither the United States Government nor any agency thereof, nor any of their employees, makes any warranty, express or implied, or assumes any legal liability or responsibility for the accuracy, completeness, or usefulness of any information, apparatus, product, or process disclosed, or represents that its use would not infringe privately owned rights. Reference herein to any specific commercial product, process, or service by trade name, trademark, manufacturer, or otherwise does not necessarily constitute or imply its endorsement, recommendation, or favoring by the United States Government or any agency thereof. The views and opinions of authors expressed herein do not necessarily state or reflect those of the United States Government or any agency thereof.

10/10/88  
10/10/88

## I. Introduction and Simulation Model

The broad sawtooth oscillations typically found in simulations of elongated, high current tokamaks affect ignition more through their effects on the plasma profiles than on the energy confinement time. Degradation of the energy confinement time is not expected unless the sawtooth mixing radius is larger than 70% of the minor radius so that more than half of the plasma volume is being disturbed. On the other hand, sawtooth oscillations have a big impact in the center of the plasma where most of the fusion power production takes place.

For plasma temperatures in the range 10 - 20 keV, the fusion power is proportional to  $\langle n^2 T^2 \rangle$ , essentially the volume average of the plasma energy squared. Clearly,  $\langle n^2 T^2 \rangle \geq (\langle nT \rangle)^2$ . The equality holds only if  $nT$  is a constant over the plasma volume as is the case with very flat profiles. In the opposite extreme of highly peaked profiles, we can maximize fusion power for a given plasma energy,  $\langle nT \rangle$ . Unfortunately, broad sawtooth oscillations cause the plasma density and temperature to remain flat on the average. A simplistic power balance at ignition implies  $\langle nT \rangle / \langle n^2 T^2 \rangle = a\tau_E$ , where  $a$  is a constant and  $\tau_E$  is the global energy confinement time. From this we can see that a nearly minimal value of  $\langle n^2 T^2 \rangle$  places the most stringent requirements on  $\tau_E$ . Conversely, we can say that flat profiles need a higher  $\langle nT \rangle$  (which forces  $\langle n^2 T^2 \rangle$  to increase) for a certain  $\tau_E$  in order to ignite.

This effect has been discussed previously in connection with the Compact Ignition Tokamak where sawtooth oscillations extending past 70% of the plasma minor radius are predicted.<sup>1</sup> In the absence of current profile control, similarly broad sawtooth oscillations should appear in INTOR and TIBER. Such sawtooth oscillations also create a large low shear region inside the  $q = 1$  surface. This leads to stability problems for both high and low mode number ballooning modes. Parameters assumed here are as in Table 1.

The 1-1/2-D BALDUR transport code<sup>2,3</sup> is used to simulate the steady-state performance of INTOR and TIBER, both in ignited and  $Q = 5$  driven modes of operation. The density, temperature, and current profiles are computed self-consistently on each flux surface. The plasma current is taken to be driven inductively since our code is not presently able to model rf current drive. Typical contours of constant toroidal flux are depicted in Fig. 1. The auxiliary heating for all simulations is, for simplicity, assumed to be equally

distributed between ions and electrons, and is taken to have a deposition profile that is centrally peaked and extends out to half of the minor radius along the midplane. A constant volume-averaged density is maintained by gas puffing. For the ignited scenarios, helium ash is removed at the appropriate rate to allow a steady-state to be maintained. Carbon is used as the primary impurity; its initial concentration is chosen to yield the value of  $Z_{eff}$  specified in Table 1.

The parameters of the thermal transport model are varied to achieve a specified level of confinement relative to the Kaye-Goldston scaling.<sup>4</sup> For the  $Q = 5$  driven mode of operation, the energy confinement time is required to be close to that predicted by the Kaye-Goldston formula (L-mode). This limit is placed at twice Kaye-Goldston (H-mode) for the ignited cases. We find that the magnitude of the sawtooth mixing radius is largely insensitive to the particular choice of the thermal transport model. In all cases, the particle diffusivity is taken to be  $D = 1/n_{e,19} \text{ m}^2/\text{s}$ , where  $n_{e,19}$  is the electron density in units of  $10^{19} \text{ m}^{-3}$ . An anomalous inward pinch velocity of  $v = 2D\tau/a^2$  is assumed to be present;  $0 \leq r \leq a$  is the half-width of a flux surface measured on the midplane. It should be noted that a smaller inward pinch would lead to flatter profiles and even more pessimistic results.

Sawtooth oscillations are modeled using a Kadomtsev reconnection picture; the period is fixed and prescribed on input. With each sawtooth crash, the particle densities and temperatures are flattened inside of the mixing region. A period of 0.5 s is used throughout; we find that the results are insensitive to moderate changes in this value. The code also has the capability of locally enhancing plasma transport in the presence of unstable high- $n$  ballooning modes. We will demonstrate that this makes ignition even more difficult.

## II. Simulation Results

The sawtooth oscillations in all simulations discussed here are very broad. Typically, the half-width on midplane of the mixing radius is  $r_{mix}/a \simeq 0.7$  for both INTOR and TIBER. In INTOR,  $q_\psi = 2.3$  at the edge so that this result is expected. Because of the high elongation used for TIBER, the safety factor is larger:  $q_\psi \simeq 4.1$ . In this case, the large mixing radius is due to the high shear near the separatrix associated with such elongations. In Fig. 2 we

show the radial and temporal variations of the ion temperature and density for the ignited INTOR simulation. Note the changes in profile due to the sawtooth oscillations.

The search in parameter space for the minimum requirements on ignition is aided by a 0-D analysis. In these calculations, profile effects on fusion power and other quantities are accounted for in a simple fashion by assuming a radial dependence  $x = x_0(1-r^2/a^2)^{\alpha_x}$ , where  $x$  represents the plasma density, temperature, or current density. In Fig. 3, contours of the auxiliary power in MW required to maintain steady-state at a given density, temperature, and level of energy confinement are plotted; the contours labeled by 0 in the upper right-hand portion of the plot represent ignited equilibrium. The parameters for the solid line contours in this 0-D calculation are taken from the ignited INTOR simulation; the "x" indicates its operating point. The profile parameters used are  $\alpha_n = 0.27$  and  $\alpha_T = 0.64$ . The dotted contours represent the same calculation but with  $\alpha_n = 1.0$  and  $\alpha_T = 1.0$ .

As a result of the sawtooth oscillations, the central values of ion density and temperature are not much larger than the volume-averaged values when averaged over a sawtooth period. Higher densities or temperatures are then required to reach ignition or  $Q = 5$  for a given confinement time. In all cases, raising the volume-averaged density appears to be the most effective remedy. As evidence, we present in Table 2 the steady-state parameters from four simulations.

For the reference confinement scaling,  $\tau_{E,KG}$ , we use an inverse quadratic combination of a neo-Alcator ohmic scaling and the Kaye-Goldston<sup>4</sup> auxiliary heated scaling:

$$\frac{1}{\tau_{E,KG}^2} = \frac{1}{\tau_{NA}^2} + \frac{1}{\tau_{AUX}^2},$$

where

$$\tau_{NA} = 7 \times 10^{-22} \bar{n}_e a R^2 q_{cyl},$$

$$\tau_{AUX} = \tau_{AUX,KG} \times \left( \frac{A_1 A_2}{A_D A_H} \right)^{0.25},$$

$$\tau_{AUX,KG} = 3.04 \times 10^{-2} \kappa^{0.28} B^{-0.09} I^{1.24} P^{-0.58} \left( \frac{\bar{n}_e}{10^{19}} \right)^{0.26} a^{-0.49} R^{1.85},$$

and

$$q_{cyl} = 5 \frac{a^2 B}{IR} \left[ \frac{1 + \kappa^2(1 + 2\delta^2)}{2} \right].$$

Here,  $\bar{n}_e$  is the line-averaged electron density in units of  $m^{-3}$ . The minor and major radii in m are denoted by  $a$  and  $R$ . The magnetic field,  $B$ , is in Tesla, and  $I$  is the plasma current in MA. The total power,  $P$ , (alpha, ohmic, and auxiliary) is in MW. The additional factor added to  $\tau_{AUX}$  represents one possible scaling for the mass dependence of the energy confinement time. In this expression,  $A_i$  is the mass of species  $i$ ; 1 and 2 refer to the main components of the plasma under consideration; D and H are for deuterium and hydrogen, respectively. The plasma elongation and triangularity are labeled by  $\kappa$  and  $\delta$ , respectively.

In the ignited runs, the total plasma  $\beta$  values correspond to Troyon coefficients of 3.9 for INTOR and 3.5 for TIBER. These are below the expected limit of 4, but are close enough for concern. Although a Murakami density limit may not apply to these experiments, we should note that all of the above cases exceed  $(n_e) = 1.5B/Rq_{cyl}$  ( $8.6 \times 10^{19} m^{-3}$  for INTOR and  $1.0 \times 10^{20} m^{-3}$  for TIBER). The 0-D calculations indicate that raising  $\tau_E$  to twice  $\tau_{E,KG}$  for the ignited scenarios will not lower the required density below this limit. In the  $Q = 5$  driven simulations, the densities may be too high to allow efficient current drive. In INTOR, this problem is further aggravated by relatively low plasma temperatures.

A high plasma current does not necessarily imply sawtooth oscillations as broad as the ones discussed above. For example, a rough simulation of an ITER design with  $R = 4.34$  m,  $a = 1.6$  m,  $\kappa = 2.0$ ,  $\delta = 0.4$ ,  $I = 18$  MA, and  $B = 4.8$  T yields  $r_{mix}/a \simeq 0.55$ . The aspect ratio,  $R/a$ , is much smaller than either INTOR or TIBER. For this reason,  $q_{cyl}$  for ITER is larger than the INTOR value despite having more than twice the current. Hence, the narrower sawtooth oscillations are expected. Since this ITER design is less elongated than TIBER, the shear near the edge is not so great. Consequently, the smaller mixing radius is again not surprising. It should be noted that this simulation still displays relatively flat profiles, with similar but less severe consequences.

The inclusion of bootstrap current may mitigate some of the effects of sawtooth oscillations. Repeating the driven TIBER simulation with bootstrap current leads to a slightly narrower mixing radius,  $r_{mix}/a \simeq 0.55$ . Consequently, the profiles are more peaked and performance improves,  $Q \simeq 5.3$ . The magnitude of these changes is consistent with the fact that bootstrap current is expected to be noticeable, but not dominant in TIBER.

### III. Stability Considerations

During a sawtooth crash, the current density and plasma pressure profiles are flattened out to the mixing radius. The pressure peaks up again on a time-scale comparable to the energy confinement time. However, the time-scale for current diffusion is much longer in these machines ( $10^2 - 10^3$  s). So, once the current is flattened by the first sawtooth crash, it tends to remain that way throughout the run. As a result, there is never any appreciable shear inside the  $q = 1$  surface. To demonstrate this effect, we show in Fig. 4 plots of the safety factor and total plasma  $\beta$  as a function of radius just prior to a sawtooth crash for the INTOR and TIBER ignited simulations.

From Fig. 4, it is clear that a significant pressure gradient exists in a very low shear region. We expect such a configuration to be unstable to various pressure-driven modes. The high- $n$  ballooning stability properties of each flux surface are calculated periodically by the BALDUR code. For this purpose, the high- $n$  ballooning mode equation is taken to be

$$\mathbf{B} \cdot \nabla \left( \frac{|\nabla\alpha|^2}{B^2} \mathbf{B} \cdot \nabla\Phi \right) + \frac{2}{B^2} \frac{\partial P}{\partial\psi} (\boldsymbol{\kappa} \cdot \mathbf{B} \times \nabla\alpha) \Phi = 0,$$

where  $\mathbf{B} = \nabla\alpha \times \nabla\psi$  is the magnetic field, and  $\psi$  is the poloidal flux divided by  $2\pi$ . The field line curvature,  $\boldsymbol{\kappa} = \frac{\mathbf{B}}{B} \cdot \nabla \left( \frac{\mathbf{B}}{B} \right)$ ;  $\Phi$  represents the perturbed electrostatic potential. Each time the equilibrium is recomputed (yielding  $\mathbf{B}$  and  $\nabla\alpha$ ), this equation is solved for the critical pressure gradient,  $\frac{\partial P}{\partial\psi}$ . We find that, in general, this critical pressure gradient is exceeded over some range of flux surfaces inside the mixing radius.

The code can be instructed to enhance transport on these flux surfaces, forcing the pressure profile to flatten and remain close to marginal stability. In Fig. 5, we demonstrate the effect of this on the temperature in the  $Q = 4.4$  simulation of TIBER. The profile remains flat, and  $\langle T_i \rangle \simeq 9.4$  keV, well below the value of 15 keV reached in the original simulation. This is also indicative of less fusion power production:  $Q \simeq 2$  for this run. In addition, the overall confinement worsens,  $\tau_E \simeq 0.6$  s  $\simeq 0.8\tau_{E,KG}$ . Hence, ignition becomes more difficult if the plasma is required to be ballooning stable across the minor radius. If narrower sawteeth are achieved, the average shear in the center will increase, allowing larger pressure gradients and greater fusion power production.

Recently, it has been discovered that the low mode number counterparts to the high-n ballooning modes can yield even smaller critical pressure gradients in low shear situations such as this.<sup>5</sup> In fact, they can be unstable under conditions in which the high-n modes would be predicted to be stable. These instabilities tend to have a large radial extent, and thus may lead to drastic changes in the plasma profile.

#### IV. Conclusions

We have demonstrated that broad sawtooth oscillations,  $r_{\text{mix}}/a \simeq 0.7$ , can arise in both INTOR and TIBER. The resulting decreases in fusion power lead to increases in the density required for ignition or  $Q = 5$  at a given level of confinement. Conversely, for a given total plasma energy the needed energy confinement time is higher. In addition, the stability properties of these plasmas are not favorable. Consequently, some form of sawtooth or current profile control would help these machines to reach their design goals.



## References

- <sup>1</sup>D. Post *et al.*, Princeton Plasma Physics Laboratory Report, PPPL-2389 (1986), (to appear in *Physica Scripta*).
- <sup>2</sup>C. Singer, D. Post, D. Mikkelsen, M. Redi, A. McKenney, A. Silverman, F. Seidl, P. Rutherford, R. Hawryluk, W. Langer, L. Foote, D. Heifetz, W. Houlberg, M. Hughes, R. Jensen, G. Lister, and J. Ogden, *Comput. Phys. Comm.*, (in press).
- <sup>3</sup>Glenn Bateman, *Algorithms for 1-1/2-D Transport*, in *Spring College on Plasma Physics, Charged Particle Transport in Plasmas*, International Centre for Theoretical Physics, Trieste, Italy, 1985.
- <sup>4</sup>S. M. Kaye and R. J. Goldston, *Nucl. Fusion* 25, 65 (1985).
- <sup>5</sup>J. Manickam, N. Pomphrey, and A. M. M. Todd, Princeton Plasma Physics Laboratory Report, PPPL-2420 (1987).

	INTOR	TIBER
minor radius (m)	1.20	0.83
major radius (m)	5.0	3.0
magnetic field (T)	5.50	5.55
plasma current (MA)	8	10
elongation	1.6	2.4
triangularity	0.25	0.40
auxiliary power (MW)	50	80
$Z_{eff}$	1.50	2.09

Table 1: Parameters for INTOR and TIBER

	INTOR I	TIBER I	INTOR II	TIBER II
$Q$	5.6	4.4	$\infty$	$\infty$
$\langle n_e \rangle (10^{20} m^{-3})$	1.4	1.4	1.6	1.6
$\langle n_D - n_T \rangle (10^{20} m^{-3})$	1.2	1.0	1.4	1.2
$n_{D0} - n_{T0} (10^{20} m^{-3})$	1.6	1.4	1.8	1.7
$\langle T_i \rangle (keV)$	8.3	15.0	11.0	17.0
$T_{i0} (keV)$	15	31	16	27
$\langle \beta_{tot} \rangle (\%)$	3.1	5.6	4.7	7.5
$P_c (MW)$	56	53	104	81
$\tau_E (s)$	1.20	0.75	1.60	1.30
$\tau_E / \tau_{E,KG}$	1.3	1.2	1.8	1.7

Table 2: Simulation results

## Figures

FIG. 1. Contour plots of equilibrium flux surfaces for (a) INTOR and (b) TIBER.

FIG. 2. Plot of ion temperature in keV, (a), and density in  $10^{20}m^{-3}$ , (b), as a function of time and radial half-width.

FIG. 3. Contour plot of auxiliary power (in MW) required in steady state for given density, temperature, and confinement as determined by a 0-D calculation. The solid contours are appropriate for the ignited INTOR simulation; its operation point is marked by the "x". The dashed contours are for parabolic density and temperature profiles.

FIG. 4. Radial dependence of the safety factor and total plasma  $\beta$  just prior to a sawtooth crash for the ignited (a) INTOR and (b) TIBER simulations.

FIG. 5. Plot of ion temperature in keV as a function of time and radial half-width for a driven TIBER simulation with enhanced transport on ballooning-unstable flux surfaces.

#87P0102

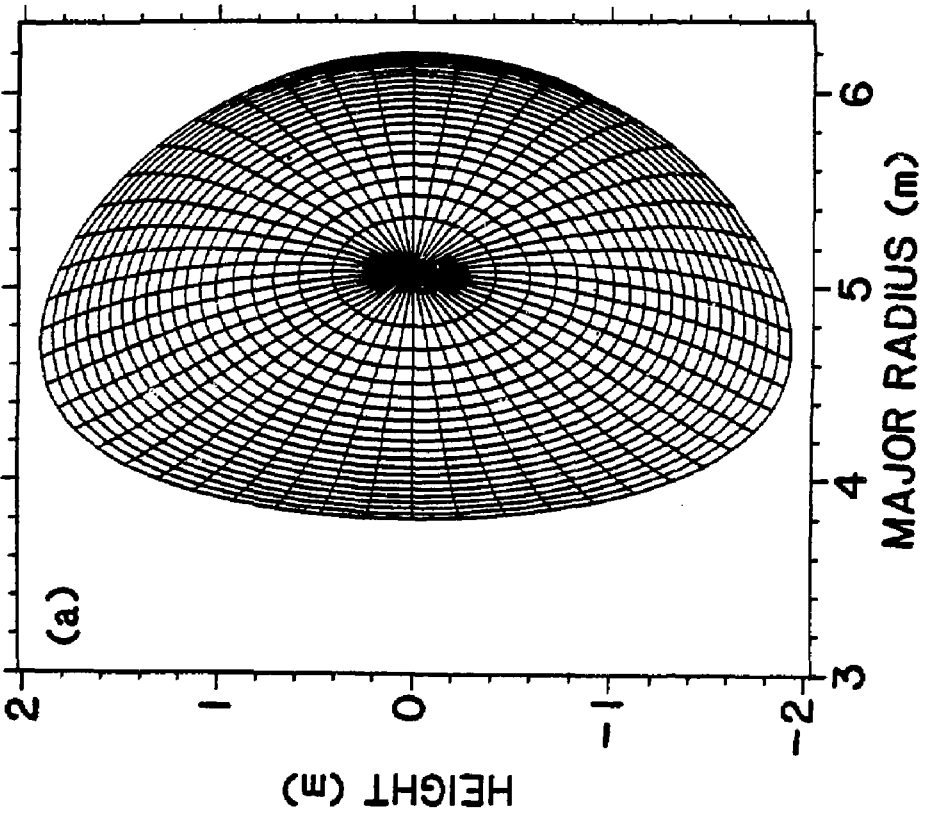
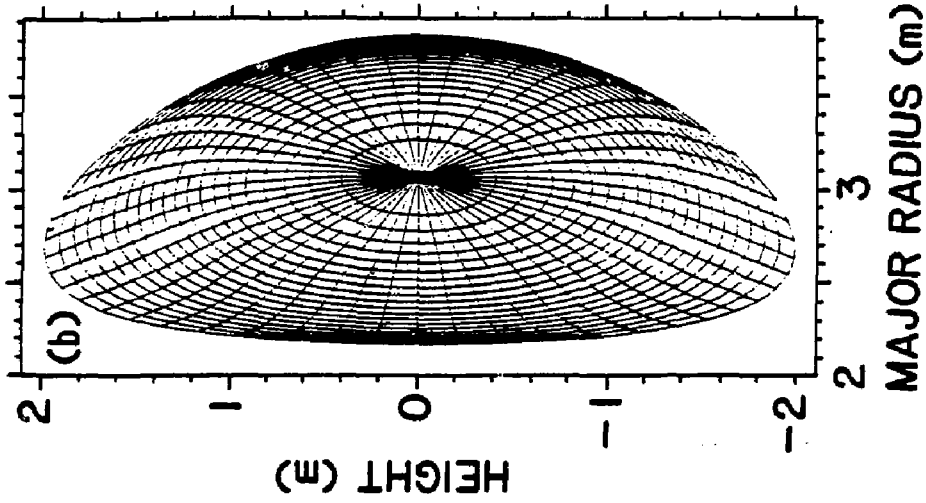


Fig. 1

#87P0105

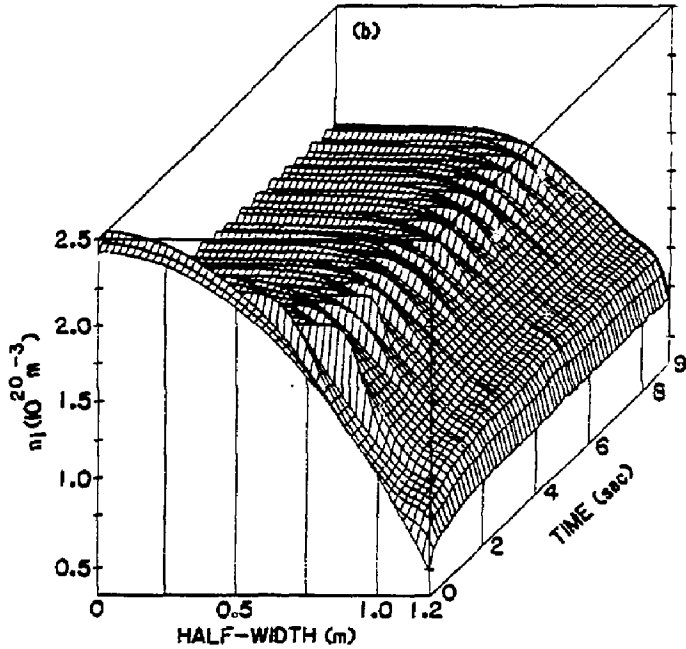
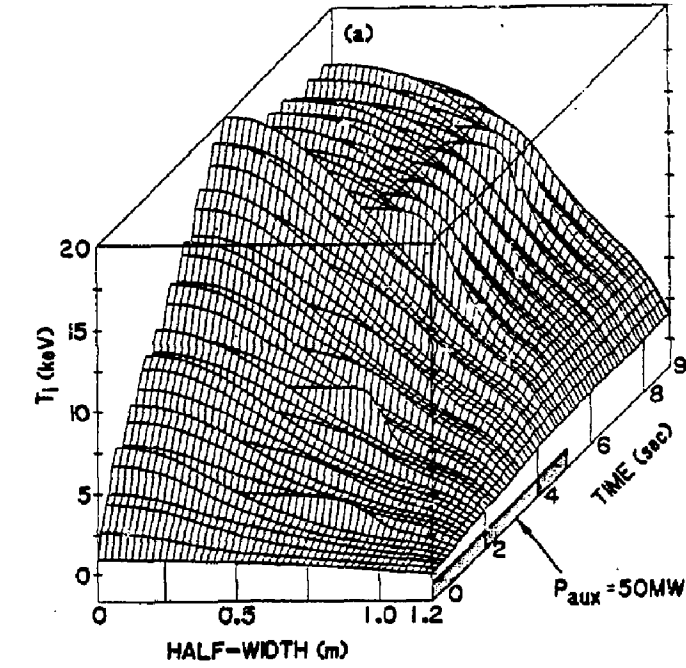


Fig. 2

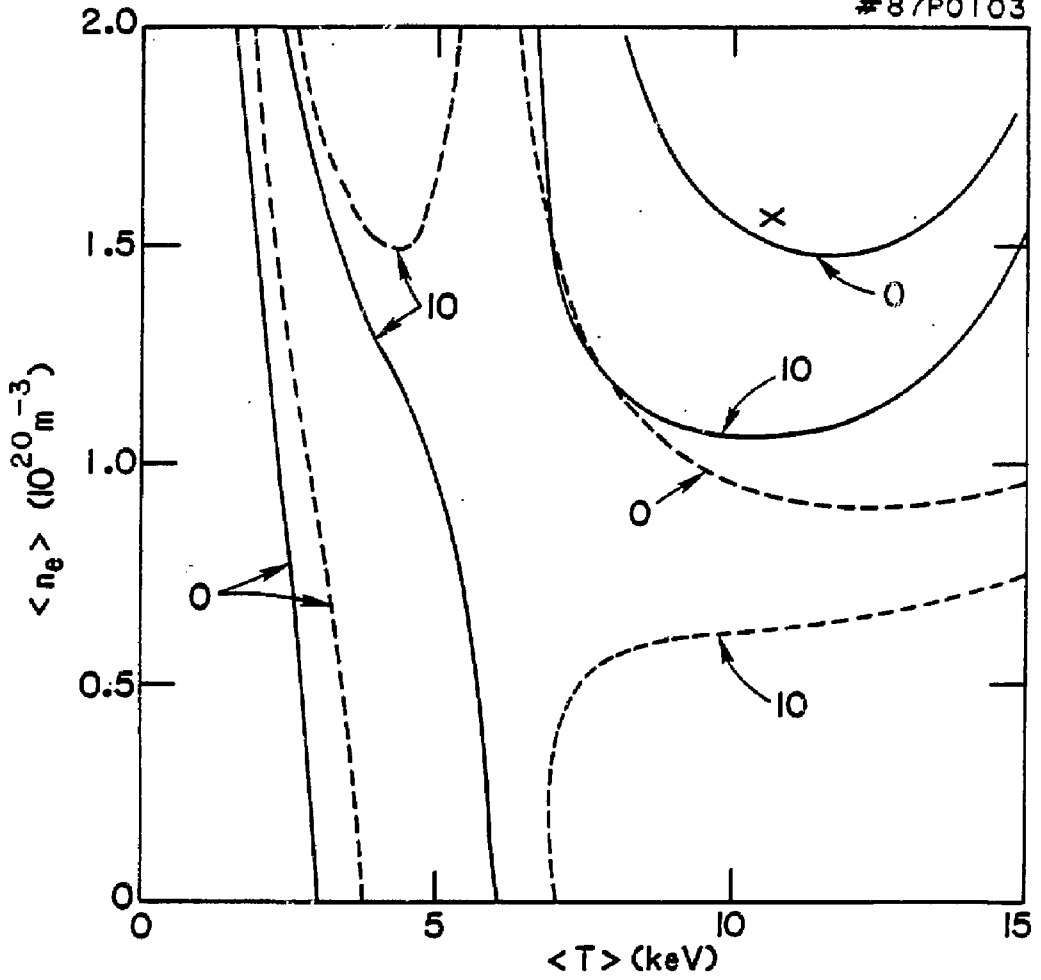


Fig. 3

#87P0110

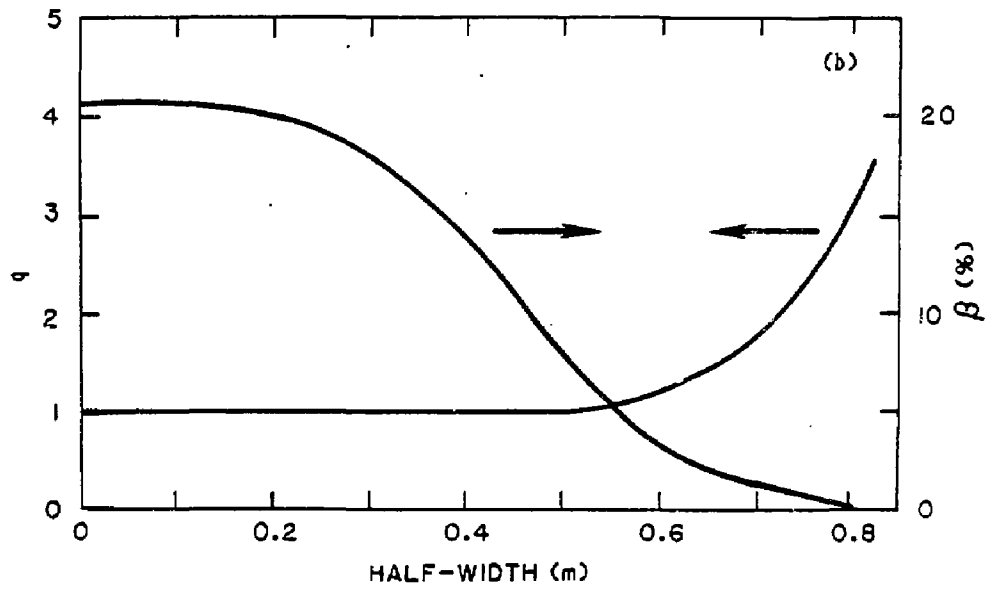
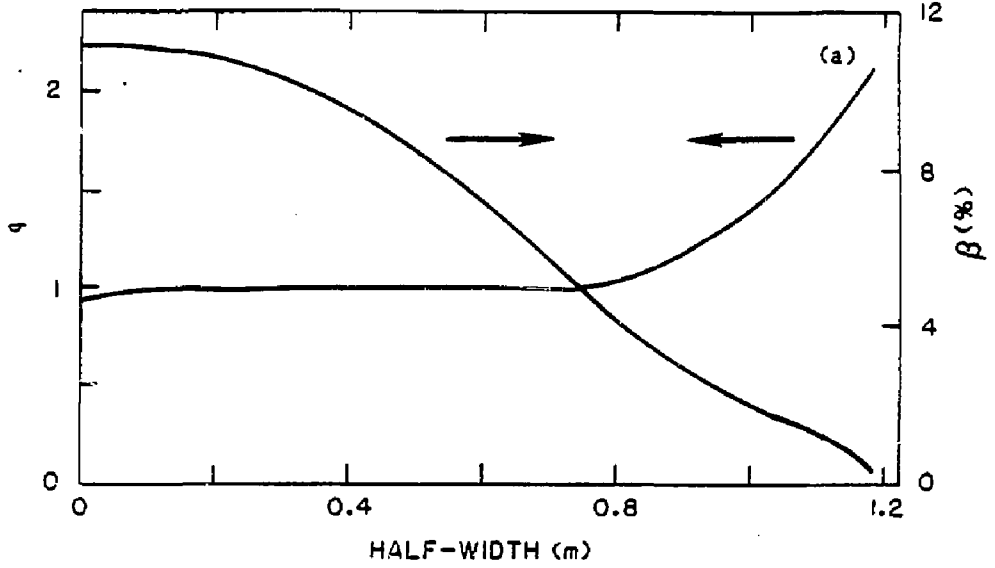


Fig. 4



#87P0104

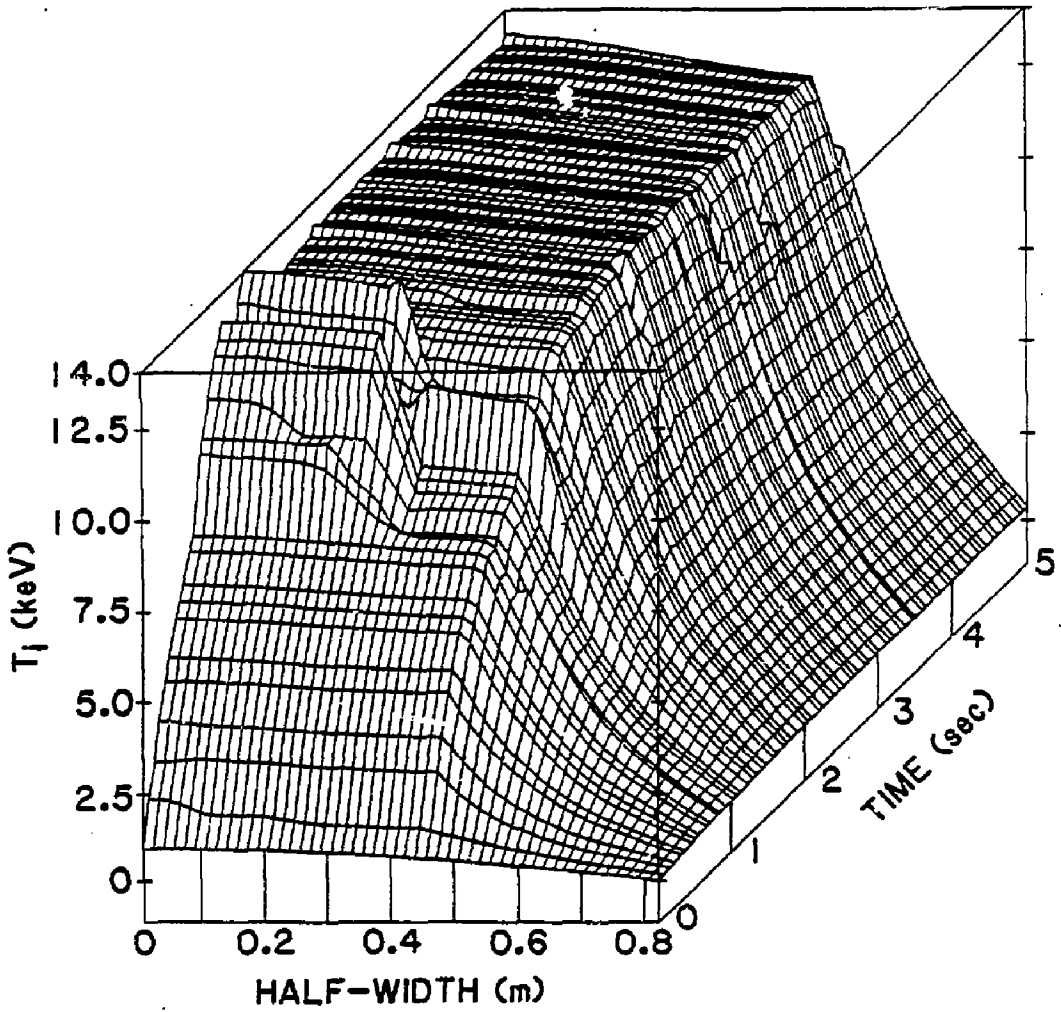


Fig. 5

EXTERNAL DISTRIBUTION IN ADDITION TO UC-20

Dr. Frank J. Paoloni, Univ of Wollongong, AUSTRALIA  
Prof. M.H. Brennan, Univ Sydney, AUSTRALIA  
Plasma Research Lab., Australian Nat. Univ., AUSTRALIA  
Prof. I.R. Jones, Flinders Univ., AUSTRALIA  
Prof. F. Cap, Inst Theo Phys, AUSTRIA  
Prof. M. Helndier, Institut für Theoretische Physik, AUSTRIA  
M. Goossens, Astronomisch Instituut, BELGIUM  
Ecole Royale Militaire, Lab de Phys Plasmas, BELGIUM  
Com. of European, Dg XII Fusion Prog, BELGIUM  
Prof. R. Boucique, Laboratorium voor Natuurkunde, BELGIUM  
Dr. P.H. Sakonaka, Univ Estadual, BRAZIL  
Instituto De Pesquisas Especiais-INPE, BRAZIL  
Library, Atomic Energy of Canada Limited, CANADA  
Dr. M.P. Bachynski, MPB Technologies, Inc., CANADA  
Dr. H.M. Skarsgard, Univ of Saskatchewan, CANADA  
Dr. H. Bernard, University of British Columbia, CANADA  
Prof. J. Telchmann, Univ. of Montreal, CANADA  
Prof. S.R. Sreenivasan, University of Calgary, CANADA  
Prof. Tudor W. Johnston, INRS-Energie, CANADA  
Dr. C.F. James, Univ. of Alberta, CANADA  
Dr. Petr Lukac, Komenskeho Univ, CZECHOSLOVAKIA  
The Librarian, Culham Laboratory, ENGLAND  
Mrs. S.A. Hutchinson, JET Library, ENGLAND  
C. Mouttet, Lab. de Physique des Milieux Ionises, FRANCE  
J. Redet, CEN/CADARACHE - Bat 306, FRANCE  
Dr. Tom Nuel, Academy Bibliographic, HONG KONG  
Preprint Library, Cent Res Inst Phys, HUNGARY  
Dr. B. Dasgupta, Sahe Inst, INDIA  
Dr. R.K. Chhajlani, Vikram Univ, INDIA  
Dr. P. Kaw, Institute for Plasma Research, INDIA  
Dr. Phillip Rosenau, Israel Inst Tech, ISRAEL  
Prof. S. Cuperman, Tel Aviv University, ISRAEL  
Librarian, Int'l Ctr-Theo Phys, ITALY  
Prof. G. Rostagni, Univ DI Padova, ITALY  
Miss Clotilde De Palo, Assoc EURATOM-ENEA, ITALY  
Biblioteca, del CNR EURATOM, ITALY  
Dr. H. Yamato, Toshiba Res & Dev, JAPAN  
Prof. I. Kawakami, Atomic Energy Res. Institute, JAPAN  
Prof. Kyoji Nishikawa, Univ of Hiroshima, JAPAN  
Direc. Dept. Lg. Tokamak Res. JAERI, JAPAN  
Prof. Satoshi Itoh, Kyushu University, JAPAN  
Research Info Center, Nagoya University, JAPAN  
Prof. S. Tanaka, Kyoto University, JAPAN  
Library, Kyoto University, JAPAN  
Prof. Nobuyuki Inoue, University of Tokyo, JAPAN  
S. Mori, JAERI, JAPAN  
M.H. Kim, Korea Advanced Energy Research Institute, KOREA  
Prof. D.I. Choi, Adv. Inst Sci & Tech, KOREA  
Prof. B.S. Lilley, University of Waikato, NEW ZEALAND  
Institute of Plasma Physics, PEOPLE'S REPUBLIC OF CHINA  
Librarian, Institute of Phys., PEOPLE'S REPUBLIC OF CHINA  
Library, Tsing Hua University, PEOPLE'S REPUBLIC OF CHINA  
Z. Li, Southwest Inst, Physics, PEOPLE'S REPUBLIC OF CHINA  
Prof. J.A.C. Cabral, Inst Superior Tech, PORTUGAL  
Dr. Octavian Petrus, AL I CUZA University, ROMANIA  
Dr. Johan de Villiers, Plasma Physics, AEC, SO AFRICA  
Prof. M.A. Hellberg, University of Natal, SO AFRICA  
Fusion Div. Library, JEN, SPAIN  
Dr. Lennart Stenflo, University of UMEA, SWEDEN  
Library, Royal Inst Tech, SWEDEN  
Prof. Hans Wilhelmson, Chalmers Univ Tech, SWEDEN  
Centre Phys des Plasmas, Ecole Polytech Fed, SWITZERLAND  
Bibliotheek, Fom-Inst voor Plasma-Fysica, THE NETHERLANDS  
Dr. D.D. Ryutov, Siberian Acad Sci, USSR  
Dr. G.A. Eliseev, Kurchatov Institute, USSR  
Dr. V.A. Glukhikh, Inst Electro-Physical, USSR  
Dr. V.T. Tolok, Inst. Phys. Tech. USSR  
Dr. L.M. Kovrizhnykh, Institute Gen. Physics, USSR  
Prof. T.J.M. Boyd, Univ College N Wales, WALES  
Nuclear Res. Establishment, Julich Ltd., W. GERMANY  
Bibliothek, Inst. Fur Plasmaforschung, W. GERMANY  
Dr. K. Schindler, Ruhr Universität, W. GERMANY  
ASDEX Reading Rm, IPP/Max-Planck-Institut für  
Plasmaphysik, W. GERMANY  
Librarian, Max-Planck Institut, W. GERMANY  
Prof. R.K. Janew, Inst Phys, YUGOSLAVIA